Supporting Information

Flexible semitransparent photovoltaic supercapacitor based on water-processed MXene electrodes

Leiqiang Qin,*[,#,a,] Jianxia Jiang,[#,a,b] Quanzheng Tao,[a] Chuanfei Wang,[a] Ingemar Persson,[a] Mats Fahlman,[a] Per O.Å. Persson,[a] Lintao Hou,[b] Johanna Rosen*[,a] and Fengling Zhang*[,a,b]

[a] Department of Physics, Chemistry and Biology (IFM), Linköping University, Linköping, SE-58183, Sweden. E-mail: leiqiang.qin@liu.se, johanna.rosen@liu.se, fengling.zhang@liu.se

[b] Guangzhou Key Laboratory of Vacuum Coating Technologies and New Energy Materials, Physics Department, Jinan University, Guangzhou, 510632, PR China

[#] These authors contributed equally to this work.

1. Calculations.

The volumetric capacitance from the cyclic voltammetry data is determined from the following equation (1):

$$C_V = \frac{1}{\Delta V}\int \frac{jdV}{s} \qquad (1)$$

C is the normalized capacitance (in units of F cm^{-3}), j is the current density (in A cm^{-3}), s is the rate (in V s^{-1}), V is the voltage (in V), ΔV is the voltage window (in V).

The volumetric specific capacitance from galvanostatic charge/discharge data is calculated from the following equation (2):

$$C_V = \frac{Idt}{vd\Delta V} \qquad (2)$$

where I and t represent the discharge current (A) and time (s), respectively; ΔV is the voltage during the discharge process after iR drop (V), v is the volume of two electrodes.

The areal capacitance C_A (F cm^{-2}) were calculated according to the following equation:

$$C_A = C_V d \qquad (3)$$

Where as d is the thickness of $Ti_3C_2T_x$ electrodes.

The Areal energy density E_A was calculated according to the following equations:

$$E_A = 0.5 C_A (\Delta V)^2 \qquad (4)$$

The overall conversion efficiency of the integrated power pack ($\eta_{overall}$) is calculated by multiplying the photoelectric conversion efficiency ($\eta_{conversion}$) in the solar cell part and energy storage efficiency ($\eta_{storage}$) in the $Ti_3C_2T_x$-based supercapacitor part from the following:

$$\eta_{overall} = \eta_{storage} \times \eta_{conversion} \qquad (5)$$

$$\eta_{overall} = E_A \times A_{SC} / (P_{in} \times t \times A_{OPV}) \qquad (6)$$

where P_{in} is the illuminated light density (100 mW cm^{-2}), t is the photo-charging time, and A_{SC} and A_{OPV} are the effective area of the $Ti_3C_2T_x$-based supercapacitor polymer-based solar cell portion of the self-powered packs, respectively.

2. Experimental Section

2.1 Preparation of $Ti_3C_2T_x$ MXene with different sizes

$Ti_3C_2T_x$ MXene was prepared by minimally intensive layer delamination method, in which selective extraction of aluminum from Ti_3AlC_2 MAX phase was done through in situ HF-forming etchant: 1 g lithium fluoride (LiF, Sigma-Aldrich, 98+%) added to 20 ml of 9 M hydrochloric acid (HCl, Sigma-Aldrich, 35-38%) and stirring for 5 min. 1 g of Ti_3AlC_2 powder was slowly added into a mixture solution, followed by stirring at 35 ˚C for 24 h. After the reaction, the product was repeatedly washed with deionized water for 6 times and centrifuged at 6000 rpm for 2 min. 20 ml of DI-water was added to the sediment, which was then subjected to vigorous shaking by hand for ~5 min. After that, the suspension was centrifuged at 1500 rpm for 30 min. The dark-green supernatant was collected with an average flake size above 1 μm. The smaller flake sizes $Ti_3C_2T_x$ was prepared by sonicating a $Ti_3C_2T_x$ colloidal solution using probe sonication with a power of 250 W at an amplitude of 40% under ice bath for 30 min. After sonication, the suspension was centrifuged at 3500 rpm for 30 min. The supernatant was collected as the small sizes $Ti_3C_2T_x$ colloidal solution.

2.2 Production of transparent, conductive films

The transparent thin films were fabricated by a spin-coating approach. Prior to the deposition of $Ti_3C_2T_x$ flakes, glass, polyethylene terephthalate (PET), or polydimethylsiloxane (PDMS) strips were treated with oxygen plasma for 2 min under vacuum (10^{-2} mbar). Then 30 μL of delaminated small size $Ti_3C_2T_x$ colloidal solution (10 mg/ml) was pipetted onto the substrate, which was fastened to the rotating plate of a spin-coater. By varying the spinning speed (ranging

from 1000 rpm to 4000 rpm), we controlled the thickness, and in turn the transmittance, of the thin films. To eliminate the trapped water among the flakes, we first annealed all the films at 100 ºC for 2 h under a high vacuum (0.1 mbar). Once the films were annealed, they were transferred into the glove box for future use.

2.3 OPV device fabrication

The conventional OPV devices based on $Ti_3C_2T_x$/glass electrodes and ITO electrode were fabricated, respectively. A PEDOT:PSS (Clevios P VP 4083) solution was spin-coated at 3000 rpm on $Ti_3C_2T_x$ electrode or ITO electrode, and dried at 110 °C for 10 min to form an anode buffer layer. Then, the solution of PM6:Y6 (1:1.2 w/w, 16 mg ml^{-1}) or PTB7-Th:$PC_{71}BM$ (1:1.5 w/w, 10 mg mL^{-1} for PTB7-Th) was spin-coated on the surfaces of buffer layers. For PM6:Y6, a thin layer of PFN-Br (0.5 mg ml^{-1} in methanol) was spin coated at 3000 r.p.m for 40 s. Finally, these samples were pumped down to a vacuum (~2×10^{-6} mbar), and an approximately 5 nm-thick LiF (only for PTB7-Th:$PC_{71}BM$) and 110 nm-thick Al electrode was deposited on top of the devices. Optical microscope (Olympus BX51) was used to define the device area (4.7 mm^2). The inverted OPV devices based on $Ti_3C_2T_x$/PET (or glass) electrodes and ITO electrode were fabricated, respectively. PEI solution (0.1%, isopropanol) was spin coated on the $Ti_3C_2T_x$ electrode or ITO electrode at 4000 rpm for 40 s followed by annealing at 110 °C for 15 min to form a cathode buffer layer. The solution of P3HT:ICBA (1:1 w/w, 20 mg ml^{-1} for P3HT) in o-dichlorobenzene was spin-coated on the surfaces of PEI at 800 rpm for 60 s in glove box followed by annealing at 130 °C for 10 min. Then the PEDOT:PSS (Clevios P VP 4083 with 0.5%/vol surface Zonyl FS 300) solution was spin coated onto the top of the photoactive layer at 2000 rpm for 60 s in atmosphere. The PDMS with $Ti_3C_2T_x$ (prepared by spin coated $Ti_3C_2T_x$ colloidal solution on PDMS at 2000 rpm for 60 s) was transfer onto PEDOT:PSS layer face down with $Ti_3C_2T_x$ contacting this layer. Then, the PDMS was slowly peeled off after annealing at 70 °C for 2 min. Finally, the transparent device was dried in vacuum. The device area is about

0.5 cm^2. For comparison, an approximately 5 nm-thick MoO_3 and 70 nm-thick Ag electrode was deposited via the thermal evaporation under high-vacuum conditions (~2×10^{-6} mbar).

2.4 Fabrication of transparent solid-state supercapacitors

(1) *Organic solid ionogel electrolyte preparation*. We employed a gel electrolyte to fabricate the solid-state transparent supercapacitors. Specifically, the precursor mixture was first prepared mixing the trimethylolpropane tris(3-mercoptopropianate) (TT), poly(ethylene glycol) diacrylate (PEGDA, M_n = 700 g/mol), and 1-ethyl-3-methylimidazolium bis(trifluoromethylsulfonyl) imide (EMIM TFSI). A stoichiometric balance between total thiol groups and (meth)acrylate groups was maintained for all samples, and ionic liquid weight percentage of 50 wt % versus the total weight of the final electrolyte precursor solution. After thorough mixing, the triethylamine (TEA) as a catalyst with 1 wt% versus the total weight of the final electrolyte precursor solution was added. The electrolyte precursor solution was then encased between two glass plates and the thickness was controlled by a 0.5 mm thick silicon wafer spacer. Freestanding ionogel films were obtained by curing the electrolyte precursor solution overnight in normal atmosphere.

(2) *Symmetric supercapacitors*. To show the potential of transparent MXene films for applications in future portable consumer electronics, symmetric solid-state supercapacitors were assembled in a sandwich-type style. Typically, the $Ti_3C_2T_x$/PET electrodes were obtained by spin-coating mothed. Then, the as-prepared ionogel electrolyte were coated on one $Ti_3C_2T_x$ /PET electrodes. Finally, two electrodes were sandwiched together face-to-face. Silver paste was added on the two electrodes to get a good contact during measurement.

2.5 Fabrication of PSC

The $Ti_3C_2T_x$-PET transparent and flexible electrode was fabricated by spin-coating method. PEI solution (0.1%, isopropanol) was spin coated on electrode at 4000 rpm for 40 s followed by annealing at 110 °C for 15 min to form a cathode buffer layer. The solution of P3HT:ICBA

(1:1 w/w, 20 mg ml^{-1} for P3HT) in o-dichlorobenzene was spin-coated on the surfaces of PEI at 800 rpm for 60 s in glove box followed by annealing at 130 °C for 10 min. Then the PEDOT:PSS (Clevios P VP 4083 with 0.5%/vol Zonyl FS 300) solution was spin coated onto the top of the photoactive layer at 2000 rpm for 60 s in atmosphere. The PDMS with $Ti_3C_2T_x$ was transfer onto PEDOT:PSS layer face down with $Ti_3C_2T_x$ contacting PEDOT:PSS. Then, the PDMS was slowly peeled off after annealing at 70 °C for 2 min. The organic ionogel electrolyte was transferred onto the $Ti_3C_2T_x$ film by lamination process. Finally, the PDMS with $Ti_3C_2T_x$ (spin coated at 2000 rpm for 60 s) was laminated onto the top of the electrolyte, and the PDMS was reserved as a protective layer of the device. Silver paste was applied onto all the $Ti_3C_2T_x$ electrode for electrical contact during the measurement.

2.6 Characterization

J-V curves were collected using a Keithley 2400 Source Meter under AM1.5 illumination provided by a solar simulator (LSH-7320 ABA LED solar simulator) with an intensity equivalent to 1,000 W m^{-2} after spectral mismatch correction. The light intensity for the J-V measurements was calibrated with a reference Si cell (VLSI standards SN 10510-0524 certified by National Renewable Energy Laboratory). EQE spectra were recorded with an integrated quantum efficiency measurement system named QE-R3011 (Enli Technology Co.), which was calibrated with a crystal silicon photovoltaic cell before use. The UPS measurement was carried out in a dedicated home designed and built spectrometer with a setting that yields a 0.08 eV width of the Fermi edge of polycrystalline gold recorded at room temperature. The UPS measurement in this work was carried out in a dedicated home designed and built spectrometer with a setting that yields an 0.08 eV width of the Fermi edge of polycrystalline gold recorded at room temperature. In the UPS measurement, the source of photons used was HeI ($h\nu = 21.2$ eV). The work function (WF) can be deduced according to WF = $h\nu$-E^{off}_{cut}, where the E^{off}_{cut} is the energy of secondary electron cut off. A Perkin Elmer Lambda 900 UV-Vis-NIR

absorption spectrometer was used for transmittance measurements. AFM was performed at ambient conditions (room temperature in a lab) using a Veeco DI Dimension 3100 scanning probe microscope, equipped with the Nanoscope IV electronics. The measurements were performed in tapping mode using Si tips (PPPNCHR-50 from Nanosensors) with a tip radius of curvature <7 nm. The thicknesses of spin-coated films were determined with a Bruker Stylus Profiler (Model: Dektak XT). The conductance measurements were performed using a Keithley 2634B SYSTEM Sourcemeter by four-point probe set-up. The conductivity measurements were performed on films that were equilibrated in a dry N_2 environment of a glovebox. The morphology and microstructure of the different electrodes were investigated by means of field emission scanning electron microscopy (LEO 1550 Gemini) equipped with energy dispersive spectroscopy (EDS). Scanning transmission electron microscopy (STEM) was performed in the Linköping double corrected FEI Titan^3 60-300, operated at 300 kV. The samples for STEM were prepared by dispersion of fine particles onto Lacey-Carbon TEM grids. XRD was carried out on a PANalytical X'Pert diffractometer using Cu Kα radiation (45 KV and 40 mA). The zeta potential and dynamic light scattering of $Ti_3C_2T_x$ MXene was tested using a Zetasizer ZEN3600 (Malvern Instruments Ltd., U.K.) The electrochemical tests were performed using a VSP potentiostat (BioLogic, France). The impedance measurements were performed with a 5 mV amplitude in a frequency range from 10 mHz to 100 kHz.

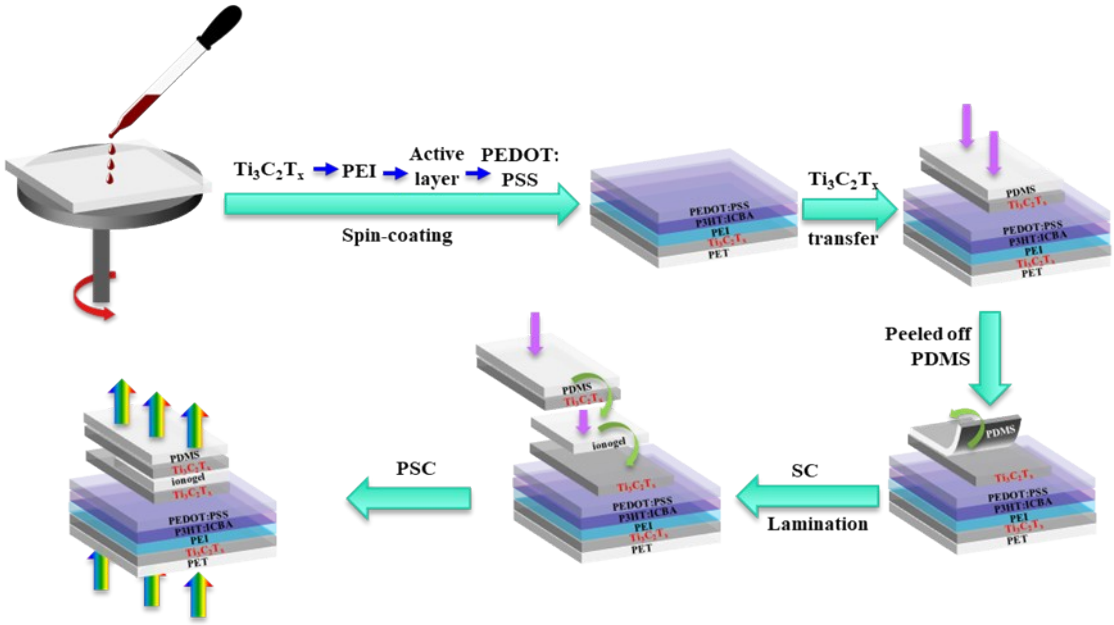

Scheme S1. The fabrication procedure of the all-solution-processed, semitransparent, flexible photovoltaic supercapacitor.

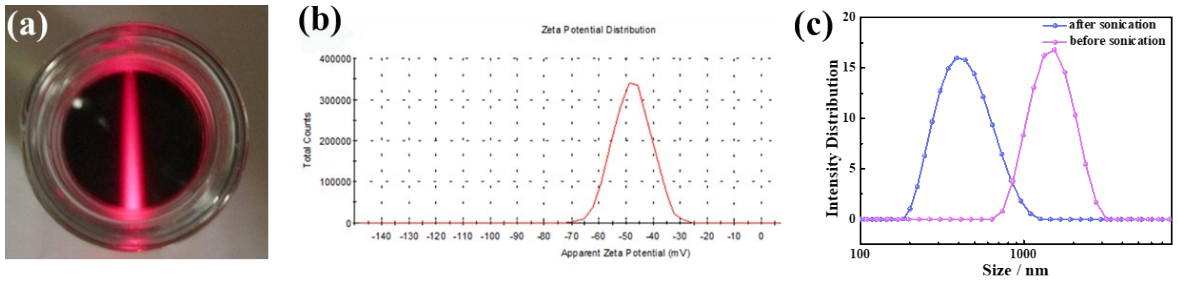

Fig. S1 (a) Digital photographs of $Ti_3C_2T_x$ colloids, displaying a clear Tyndall scattering effect with laser light. (b) Zeta potentioal of the $Ti_3C_2T_x$ colloids. The surfaces of the $Ti_3C_2T_x$ sheets are shown to be negatively charged with a zeta-potential of -47.7 mV. (c) Dynamic light scattering (DLS) intensity distribution of $Ti_3C_2T_x$ with different flake sizes. The size distribution of $Ti_3C_2T_x$ flakes was estimated using dynamic light scattering (DLS). The data show that the flake sizes of $Ti_3C_2T_x$ after sonication in the range of 200 to 900 nm, with an average size of ~400 nm. In comparison, the flake sizes of $Ti_3C_2T_x$ before sonication ranges from 1 to 3 μm, with an average size of 1.7 μm.

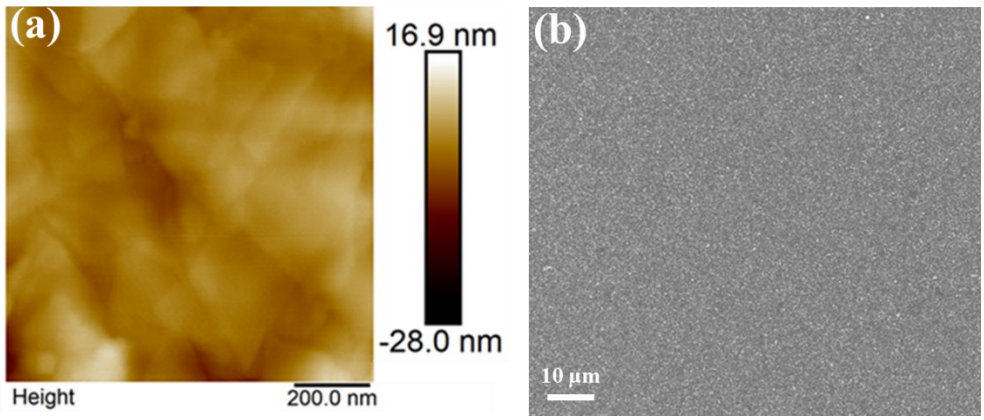

Fig. S2 (a) The AFM image of $Ti_3C_2T_x$ files by spin-coating on glass substrate at 2000 RPM with the RMS of 2.93 nm. (b) the surface SEM image of $Ti_3C_2T_x$ films by spin-coating on glass substrate at 2000 RPM.

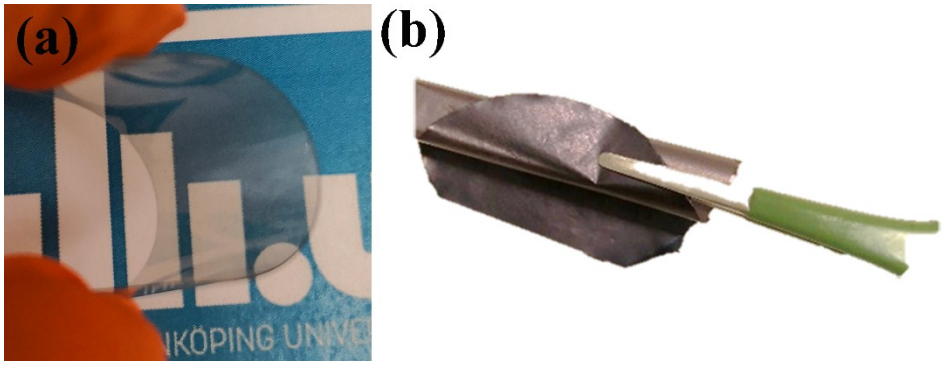

Fig. S3 Photo image of (a) flexible, transparent $Ti_3C_2T_x$ film on PET substrate and (b) flexible $Ti_3C_2T_x$ film by filtration method (thickness about 10 µm).

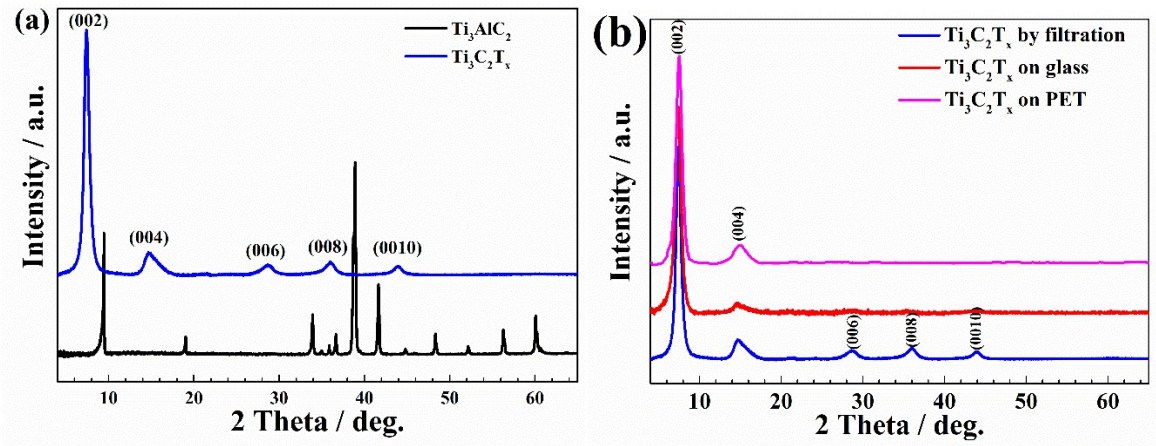

Fig. S4 (a) X-ray diffraction (XRD) patterns of Ti_3AlC_2 MAX phase and $Ti_3C_2T_x$ films by filtration (~ 10 μm). (b) X-ray diffraction (XRD) patterns of Ti3C2Tx film prepared by filtration and spin-coating on glass or PET. The X-ray diffraction (XRD) patterns of spin-coated $Ti_3C_2T_x$ films on glass and poly(ethylene terephthalate) (PET) show a sharp (002) peak, which is comparable to the filtrate film, suggesting the high degree of alignment of flakes parallel to the substrate plane under the effect of the shear force.

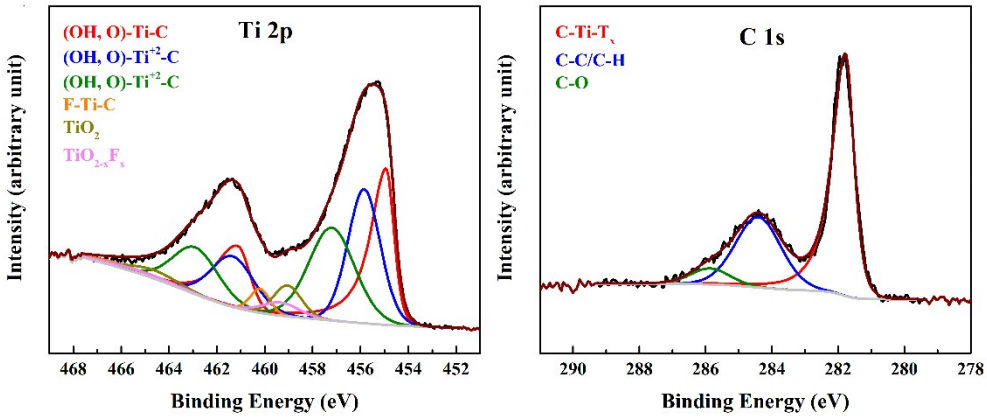

Fig. S5 High-resolution XPS spectra of $Ti_3C_2T_x$.

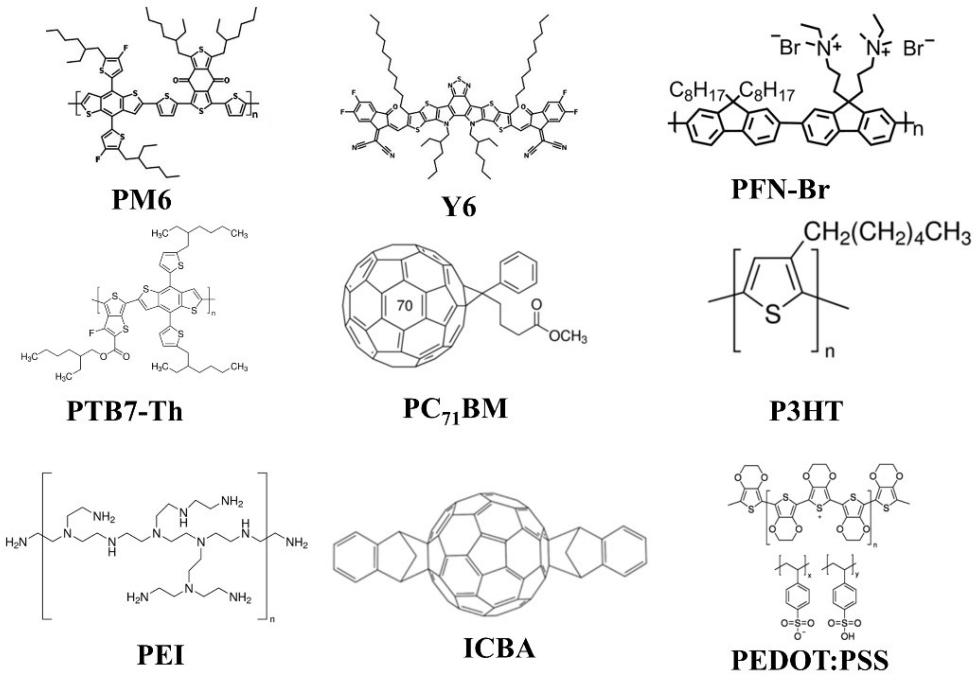

Fig. S6 Molecular structures of photoactive layer and interface materials.

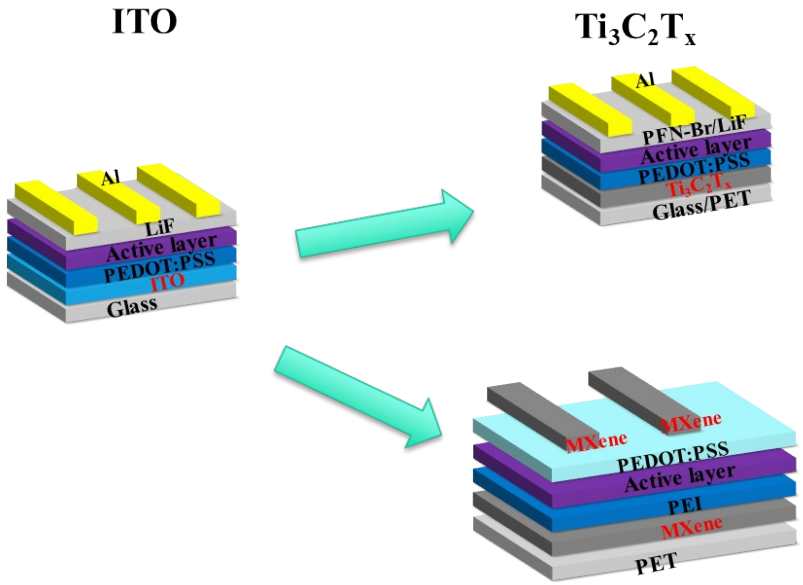

Fig. S7 The device architecture of different electrode structures.

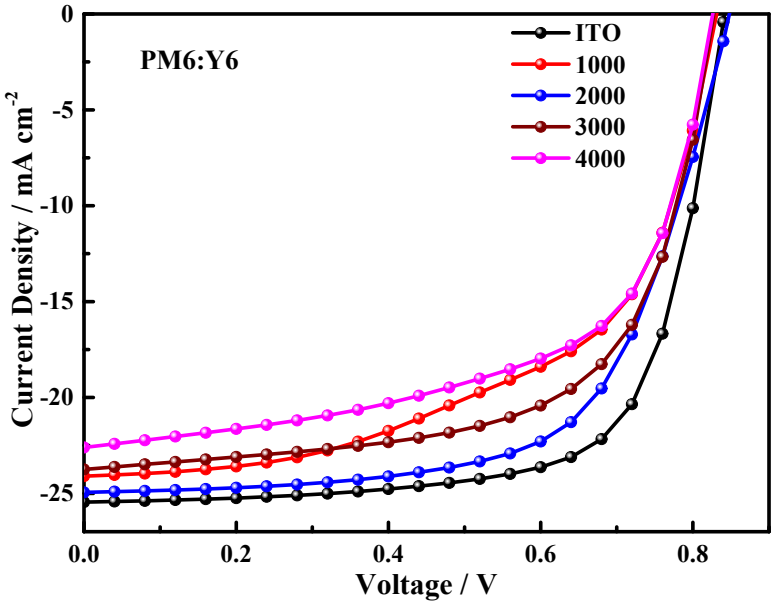

Fig. S8 *J-V* curves of the OPVs with $Ti_3C_2T_x$ electrodes prepared at different rotating speed by spin-coating method, ITO electrode as control devices. PM6:Y6 as the active layer, measured under AM1.5G 100 mW cm^{-2} illumination.

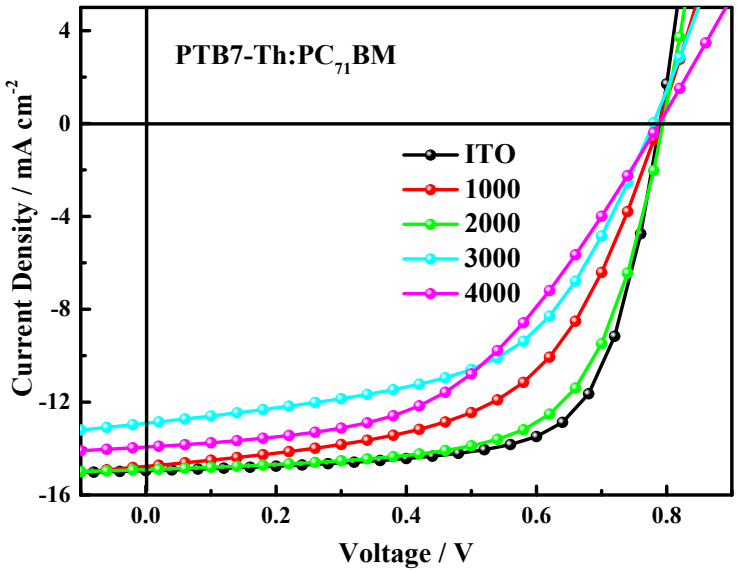

Fig. S9 *J-V* curves of the OPVs with $Ti_3C_2T_x$ electrodes prepared at different rotating speed by spin-coating method, ITO electrode as control devices. PTB7-Th:$PC_{71}BM$ as the active layer, measured under AM1.5G 100 mW cm^{-2} illumination.

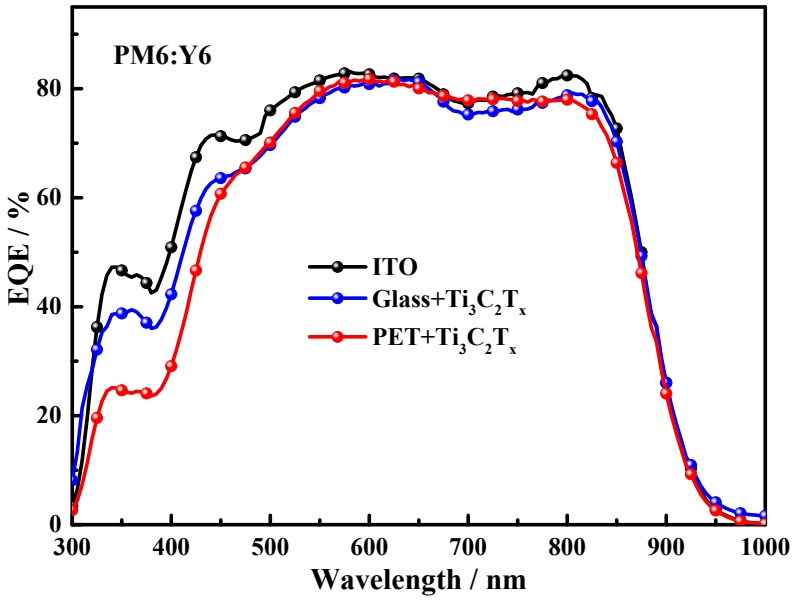

Fig. S10 EQE spectra of OPV devices based on PM6:Y6 active layer with ITO or $Ti_3C_2T_x$ as elecreodes.

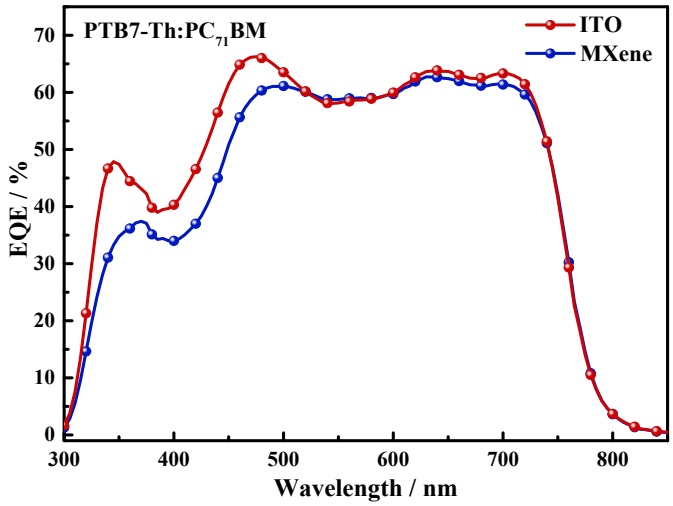

Fig. S11 EQE spectra of OPV devices based on PTB7-Th:$PC_{71}BM$ active layer with ITO or $Ti_3C_2T_x$ as elecreodes.

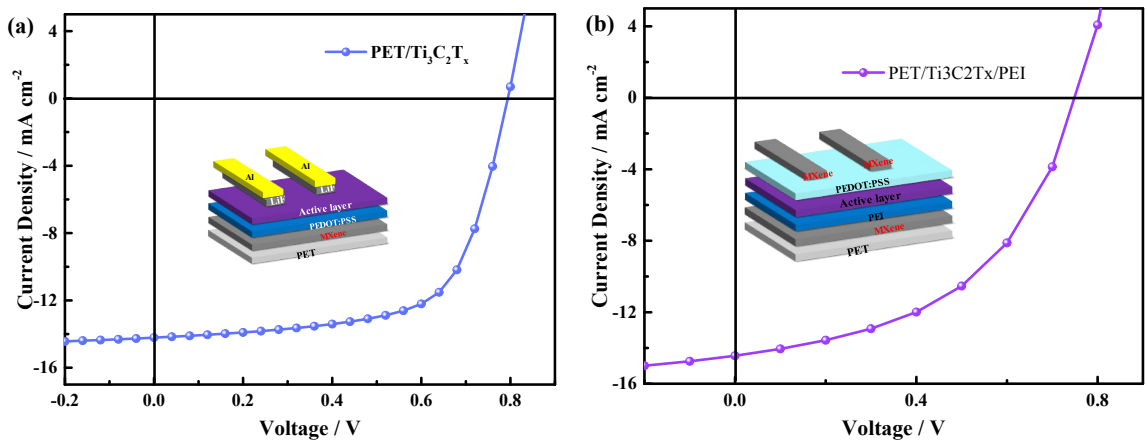

Fig. S12 J-V curves of the OPV devices with a configuration of (a) PET/$Ti_3C_2T_x$/PEDOT:PSS/PTB7-Th:$PC_{71}BM$/LiF/Al and (b) PET/$Ti_3C_2T_x$/PEI/PTB7-Th:$PC_{71}BM$/PEDOT:PSS/$Ti_3C_2T_x$.

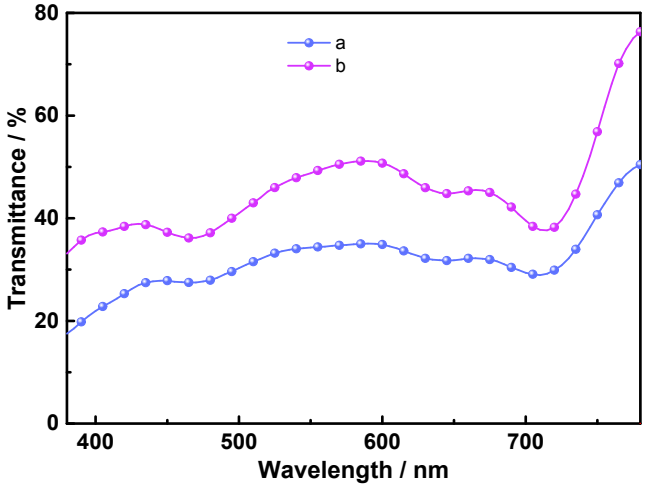

Fig. S13 Transmittance spectra of (a) PET/$Ti_3C_2T_x$/PEI/PTB7-Th:$PC_{71}BM$/PEDOT:PSS/$Ti_3C_2T_x$ device, (b) glass/$Ti_3C_2T_x$/PTB7-Th:$PC_{71}BM$.

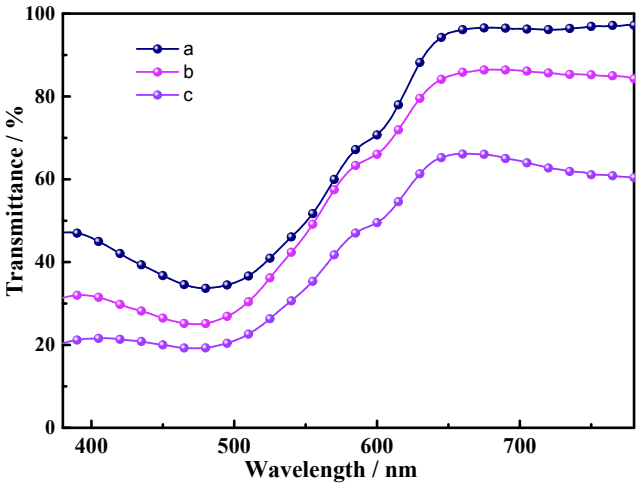

Fig. S14 Transmittance spectra of (a) glass/$Ti_3C_2T_x$/P3TH:ICBA, (b) ITO/PEI/P3TH:ICBA/PEDOT:PSS/$Ti_3C_2T_x$ device, (c) glass/$Ti_3C_2T_x$/PEI/P3TH:ICBA/PEDOT:PSS/$Ti_3C_2T_x$ device.

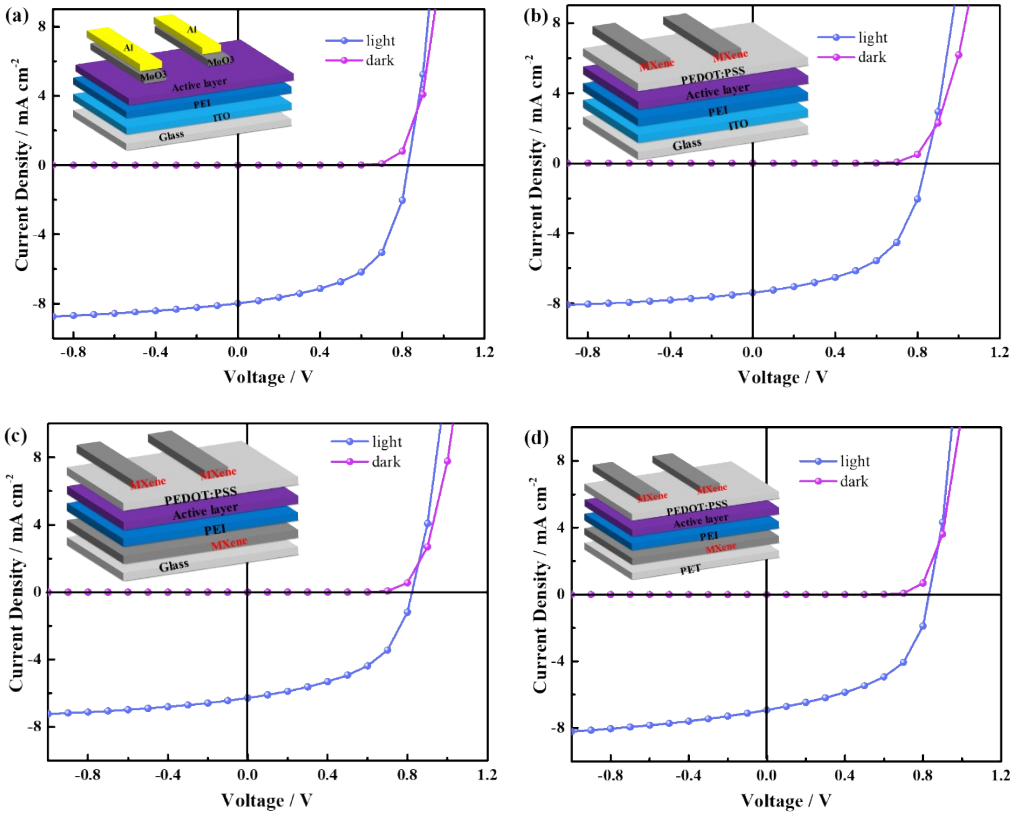

Fig. S15 Light and dark current of the OPV devices with a configuration of (a) ITO/PEI/P3TH:ICBA/MoO_3/Al, (b) ITO/PEI/P3TH:ICBA/PEDOT:PSS/$Ti_3C_2T_x$, (c) glass/$Ti_3C_2T_x$/PEI/P3TH:ICBA/PEDOT:PSS/$Ti_3C_2T_x$, and (d) PET/$Ti_3C_2T_x$/PEI/P3TH:ICBA/PEDOT:PSS/$Ti_3C_2T_x$.

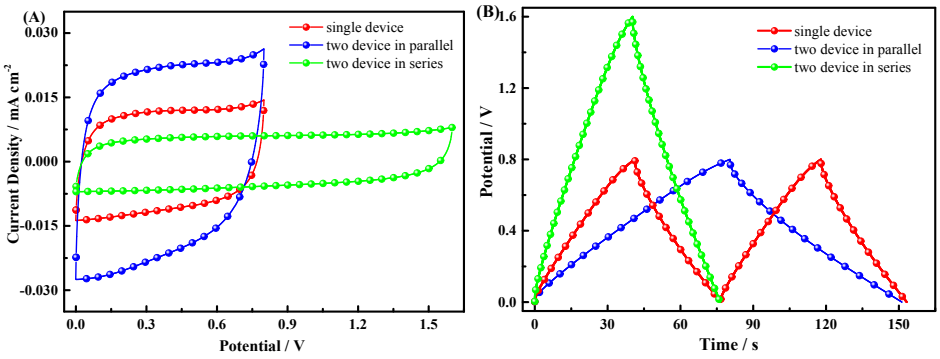

Fig. S16 (A) CV curves of the devices connected in series and in parallel at a scan rate of 100 mV s^{-1}. A single device is shown for comparison. (B) GCD curves of devices connected in series and in parallel at a current density of 10 A cm^{-3}.

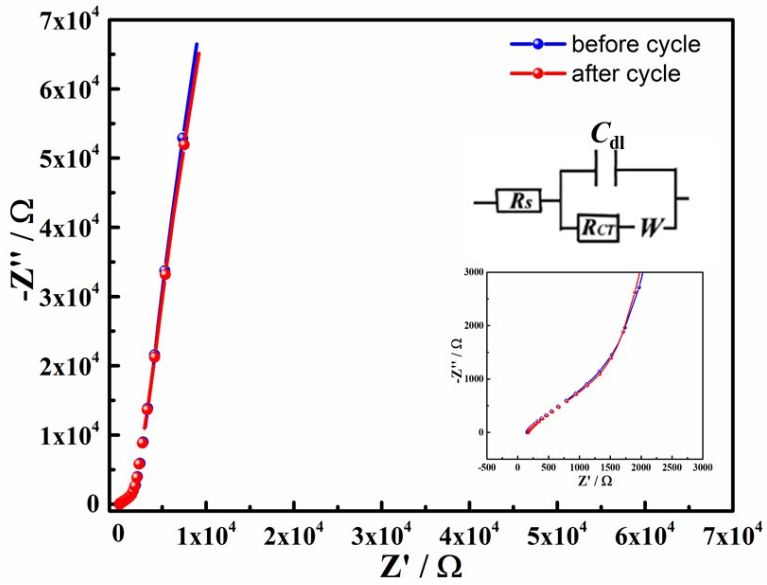

Fig. S17 Electrochemical impedance spectroscopy data of $Ti_3C_2T_x$ devices tested at the opencircuit potential within the frequency range from 10^{-1} to 10^5 Hz before and after cycling test. Inset: up is the Randles equivalent circuit, down is the enlarged plot in the high frequency region.

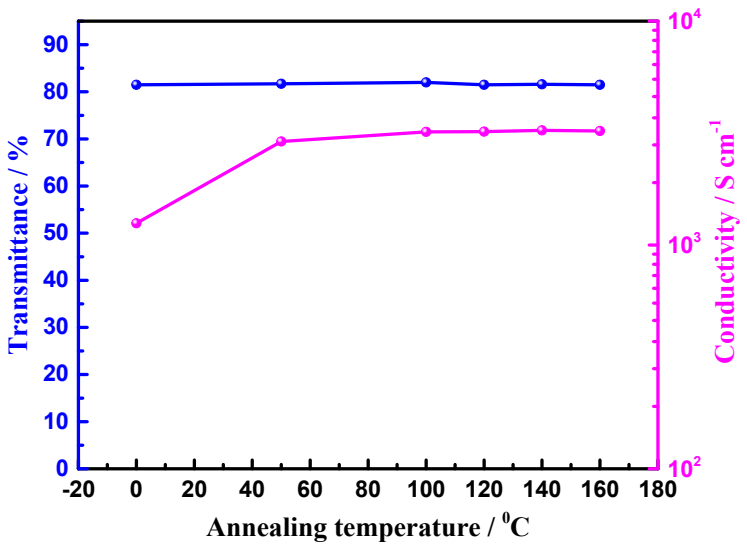

Fig. S18 The transmittance and conductivity of the MXene film (spin coating at 2000 RPM) at different annealing temperature.

To eliminate the trapped water among the flakes, we have annealed all the films at 100 ºC for 2 h under a high vacuum (0.1 mbar) before use. Therefore, annealing can improve the conductivity of the film, but has no effect on the transmittance.

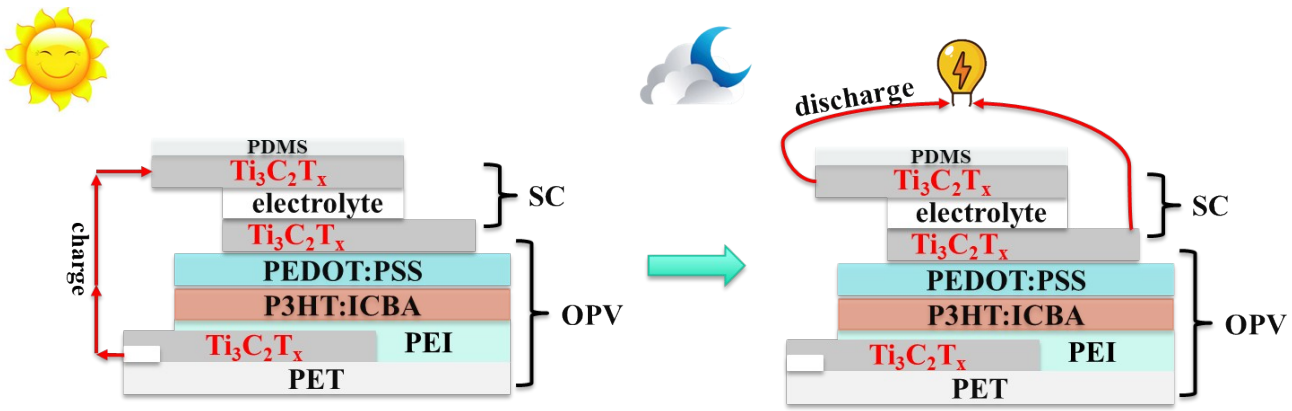

Fig. S19 The working principle of the semitransparent, flexible photovoltaic supercapacitor.

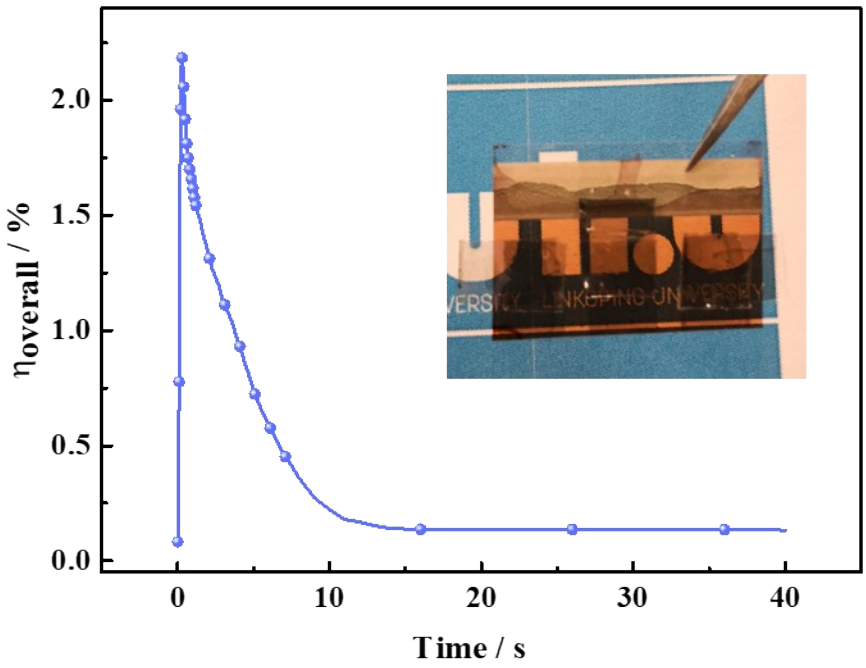

Fig. S20 Overall photoelectric conversion on the photocharging time of PSC devices. Inset: photograph of transparent, flexible PSC device based on $Ti_3C_2T_x$ electrodes.

Table S1. Photovoltaic performance parameters of the OPVs with different electrodes under AM1.5G 100 mW cm^{-2} illumination.

Active layer	RPM	Thickness [nm]	J_{sc} [mA cm^{-2}]	V_{oc} [V]	FF [%]	PCE [%]
PM6:Y6	ITO	-	25.46	0.84	70.3	15.07
	4000	9	22.61	0.83	59.2	11.07
	3000	12	23.75	0.83	63.6	12.52
	2000	17	24.97	0.84	64.9	13.62
	1000	34	24.1	0.83	56.2	11.26
PTB7-Th:$PC_{71}BM$	ITO	-	14.95	0.79	69.79	8.24
	4000	9	13.93	0.79	49.08	5.39
	3000	12	14.26	0.79	55.58	6.47
	2000	17	14.91	0.79	65.61	7.76
	1000	34	12.91	0.78	54.16	5.45

Table S2. State-of-the-art PCE performances of flexible OPV devices in literatures.

Transparent electrodes	Preparation Method	Active layer	PCE [%]	Refs
PEDOT:PSS	Solution process	P3HT:$PC_{71}BM$	2.87	1
Graphene	Transferring	PTB7:$PC_{71}BM$	7.2	2
CNTs	Solution process	PTB7:$PC_{71}BM$	3.91	3
Ag meshes/ PEDOT:PSS	Printing/ Solution process	PTB7:$PC_{71}BM$	6.73	4
ZnO/Cu(9.5 nm) on Cu(O)/ZnO	Magnetron sputtering	PTB7:$PC_{71}BM$	7.7	5
PEDOT:PSS	Solution process	PTB7-Th:$PC_{71}BM$	7.7	6
AgNWs	Solution process	PTB7-Th:$PC_{71}BM$	8.75	7
AgNWs	Solution process	PTB7-F20:PC71BM	5.02	8
PEDOT:PSS	Solution process	PBDTT-S-TT:PC71BM	6.42	9
PEDOT:PSS	Solution process	PBDB-T:IT-M	10.12	10
ITO	Magnetron sputtering	PBDTTTOFT:PC71BM	10.49	11
ITO	Commercialization	PCE10:IEICO-4F	12.5	12
Glass/$Ti_3C_2T_x$	**Solution process**	**PM6:Y6**	**13.62**	**This work**
PET/$Ti_3C_2T_x$	**Solution process**	**PM6:Y6**	**13.15**	

Reference:

[1] B. J. Worfolk, S. C. Angrews, S. Park, J. Reinspach, N. Liu, M. F. Toney, S. C. B. Mannsfeld, Z. Bao, Proc. Natl. Acad. Sci. 2015, 112, 14138.

[2] H. Park, S. Chang, X. Zhou, J. Kong, T. Palacios, S. Gradecak, Nano Lett. 2014, 14, 5148.

[3] I. Jeon, K. Cui, T. Chiba, A. Anisimov, A. G. Nasibulin, E. I. Kauppinen, S. Maruyama, Y. Matsuo, J. Am. Chem. Soc. 2015, 137, 7982.

[4] W. Kim, S. Kim, I. Kang, M. S. Jung, S. J. Kim, J. K. Kim, S. M. Cho, J.-H. Kim, J. H. Park, ChemSusChem 2016, 9, 1042.

[5] G. Zhao, M. Song, H.-S. Chung, S. M. Kim, S.-G. Lee, J.-S. Bae, T.-S. Bae, D. Kim, G.-H. Lee, S. Z. Han, H.-S. Lee, E.-A. Choi, J. Yun, ACS Appl. Mater. Interfaces 2017, 9, 38695.

[6] N. Kim, H. Kang, J.-H. Lee, S. Kee, S. H. Lee, K. Lee, Adv. Mater. 2015, 27, 2317.

[7] J. H. Seo, I. Hwang, H.-D. Um, S. Lee, K. Lee, J. Park, H. Shin, T.-H. Kwon, S. J. Kang, K. Seo, Adv. Mater. 2017, 29, 1701479.

[8] M. Song, D. S. You, K. Lim, S. Park, S. Jung, C. S. Kim, D.-H. Kim, D.-G. Kim, J.-K. Kim, J. Park, Y.-C. Kang, J. Heo, S.-H. Jin, J. H. Park, J.-W. Kang, Adv. Funct. Mater. 2013, 23, 4177.

[9] X. Fan, B. Xu, S. Liu, C. Cui, J. Wang, J, Wang, F. Yan, ACS Appl. Mater. Interfaces 2016, 8, 14029.

[10] W. Song, X. Fan, B. Xu, F. Yan, H. Cui, Q. Wei, R. Peng, L. Hong, J. Huang, Z. Ge, Adv. Mater. 2018, 30, 1800075.

[11] S. Park, S. W. Heo, W. Lee, D. Inoue, Z. Jiang, K. Yu, H. Jinno, D. Hashizume, M. Sekino, T. Yokota, K. Fukuda, K. Tajima, T. Someya, Nature 2018, 561, 516.

[12] S. Xiong, L. Hu, L. Hu, L. Sun, F. Qin, X. Liu, M. Fahlman, Y. Zhou, Adv. Mater. 2019, 31, 1806616.